Remote Sensing of Environment 143 (2014) 180–191

Contents lists available at ScienceDirect

Remote Sensing of Environment

journal homepage: www.elsevier.com/locate/rse

Rapidly accelerating subsidence in the Greater Vancouver region from two decades of ERS-ENVISAT-RADARSAT-2 DInSAR measurements

Sergey V. Samsonov [a,*], Nicolas d'Oreye [b,c], Pablo J. González [d], Kristy F. Tiampo [d], Leila Ertolahti [e], John J. Clague [e]

[a] Natural Resources Canada, 588 Booth Street, Ottawa, ON K1A0Y7, Canada
[b] European Center for Geodynamics and Seismology, Rue Josy Welter 19, L-7256 Walferdange, Luxembourg
[c] National Museum of Natural History, Dept. Geophysics/Astrophysics, Rue Josy Welter 19, L-7256 Walferdange, Luxembourg
[d] Department of Earth Sciences, Western University, Biological and Geological Sciences Building, 1151 Richmond Street, London, ON, N6A5B7, Canada
[e] Department of Earth Sciences, Simon Fraser University, 8888 University Drive, Burnaby, BC, V5R1S6, Canada

ARTICLE INFO

Article history:
Received 7 June 2013
Received in revised form 23 December 2013
Accepted 23 December 2013
Available online 31 January 2014

Keywords:
Greater Vancouver Region
Fraser River Delta
Rapid ground subsidence
Ground deformation
InSAR
MSBAS

ABSTRACT

Rapidly accelerating ground subsidence in the south-western part of British Columbia, the third largest metropolitan area in Canada with over 2.3 million of inhabitants, is estimated using the Multidimensional Small Baseline Subset (MSBAS) advanced Differential Interferometric Synthetic Aperture Radar (DInSAR), an effective processing strategy for multi-mission, multi-temporal SAR data. The Synthetic Aperture Radar (SAR) data used in this study consists of seven independent data sets: one ascending and one descending ERS-1/2 and ENVISAT frames, together spanning July 1995–September 2010, and three RADARSAT-2 frames spanning February 2009–October 2012. During the July 1995–October 2012 period we observe fast ground subsidence with a maximum rate of about 2 cm/year in the Greater Vancouver region that includes the Fraser River Delta and the cities of Burnaby, Richmond, Surrey, New Westminster and Vancouver. The rapidly accelerating subsidence is observed beneath the Vancouver International Airport, SkyTrain terminal as well as several agricultural and industrial locales. These time series suggest that the subsidence rate at the studied regions does not decrease with time, as suggested in previous studies, but remains steady or increases. These results also demonstrate the importance of acquiring and appropriately estimating longer time series, as previous studies on the same Greater Vancouver area may have misinterpreted the long term ground deformation rate and direction and underestimated the potential hazard. The long term impact of this subsidence on urban infrastructure can be significant and needs to be investigated further.

1. Introduction

Over 85% of the world river deltas are affected by subsidence as a result of sediment compaction due to removal of groundwater, oil and gas from the delta's underlying sediments as well as the trapping of the sediments by dams in the reservoirs upstream (Syvitski et al., 2009). Close to half a billion people live on or near deltas characterized by flat terrains suitable for urban development. Subsidence occurring over a long time is damaging to urban infrastructure, including highways, subways and railways, buildings, and underground gas, water, electricity and sewage systems (Dong, Samsonov, Yin, Ye, & Cao, 2013). Area vulnerable to flooding due to subsidence and relative sea level rise is expected to increase by 50% from 260,000 km^2 during the twenty first century (Syvitski et al., 2009).

The Greater Vancouver region is located along Fraser River delta in the southwestern part of British Columbia in Canada. This region consists of the cities of Burnaby, Richmond, Surrey, New Westminster and Vancouver and is the third largest metropolitan area in Canada, with over 2.3 million of inhabitants. Due to its particular location and geological environment this area is susceptible to various natural hazards including earthquake ground motion and liquefaction, flooding, slope instabilities and landslides. Ground subsidence in this region was reported by Mazzotti, Lambert, van der Kooij, and Mainville (2009). During 1992–1999 they observed slow, widespread subsidence beneath city of Richmond. The cause of this subsidence was attributed to sediment consolidation under the anthropogenic and natural loading. It also was suggested that the rate of subsidence should decrease over time due to relaxation.

In order to study the long-term (1995–2012) subsidence in the Greater Vancouver region we applied advanced Differential Interferometric Synthetic Aperture Radar (DInSAR) (Hooper, Bekaert, Spaans, & Arkan, 2012; Massonnet & Feigl, 1998; Rosen et al., 2000) capable of achieving sub-centimeter precision and high spatial resolution over a large area. A DInSAR product or interferogram is calculated from two SAR images acquired by space- and/or air-borne sensors with identical characteristics at two different times and captures the associated deformation. Spatial resolution of the modern SAR sensors ranges from 1 to

* Corresponding author at: Research Scientist, Natural Resources Canada, 588 Booth Street, Ottawa, ON K1A0Y7, Canada.Tel: +1 613 995 4913; fax: +1 613 947 1385.
E-mail address: sergey.samsonov@nrcan-rncan.gc.ca (S.V. Samsonov).

0034-4257/$ – see front matter.
http://dx.doi.org/10.1016/j.rse.2013.12.017

20 m over areas from 10 × 10 km to 300 × 300 km, normally resulting in an inverse relation between resolution and coverage. For modern satellite constellations the repeat cycle ranges from one day to a few weeks, but the typical repeat cycle for a single satellite mission ranges from 24 to 41 days.

Repeatedly acquired SAR data from a single sensor can be used to obtain the Line-of-Sight (LOS) time series of ground deformation (Berardino, Fornaro, & Lanari, 2002; Ferretti, Novali, Burgmann, Hilley, & Prati, 2004; Ferretti, Prati, & Rocca, 2001; Hooper, 2008; Samsonov, van der Koij, & Tiampo, 2011; Usai, 2003). The results of this classical technique, however, are limited to the time period of the particular data set and do not distinguish horizontal and vertical motion. Decomposition of static DInSAR LOS measurements into two (skipping north–south) or three components of displacement vector has been discussed in Rocca (2003), Wright, Parsons, and Lu (2004).

In order to overcome limitations facing classical techniques and to produce continuous, multidimensional and dynamic solution (time series), we developed the Multidimensional Small Baseline Subset (MSBAS) technique (Samsonov & d'Oreye, 2012) that combines multiple DInSAR data into a single solution with improved characteristics, lower noise and denser temporal resolution. Assuming that individual ascending and descending data sets overlap in time, the MSBAS produces a single time series with uninterrupted temporal coverage. This methodology addresses data redundancy and multidimensionality problems by decomposing LOS DInSAR measurements into the vertical and horizontal (mainly east–west) time series of ground deformation using ascending and descending DInSAR data. The MSBAS technique was successfully used to study coal-mining related subsidence in the Greater Luxembourg region (Samsonov, d'Oreye, & Smets, 2013), potash-mining related subsidence in Saskatchewan (Samsonov, González, Tiampo, & d'Oreye, 2013a; Samsonov, González, Tiampo, & d'Oreye, 2013b) and groundwater-extraction related subsidence in the Bologna region of Italy (Samsonov, González, & Tiampo, 2014). The MSBAS time series analysis revealed, with remarkable accuracy, seasonal oscillations at summit of Vesuvius, 2005–2013 inflation of Campi Flegrei (Samsonov, González, Tiampo, Camacho, & Fernández, 2014) and pre-eruptive deformation at Nyamulagira volcano (Smets et al., 2014).

Deformation maps for the Greater Vancouver region presented here were calculated from nearly two decades of SAR measurements, spanning 1995–2012 and consisting of over eight hundred interferograms from three different SAR sensors (ERS-1/2, ENVISAT, and RADARSAT-2). We demonstrate that the application of a classical time series method using a data set of only seven years in duration may lead to erroneous conclusions about the long term ground deformation. Results from classical DInSAR time series methods are rarely challenged. With the launch in the near future of many new sensors (ALOS-2, Sentinel 1A and 1B, PAZ, RCM, CSK-second generation), this study will be of a particular interest to the research community as an example of an effective and superior strategy for processing multi-mission, multi-temporal SAR data.

2. Processing methodology

The theoretical derivation of the MSBAS technique was described in detail in Samsonov and d'Oreye (2012) and here we discuss only computational aspects, assumptions, and error analysis that were not addressed in the previous studies. The MSBAS method that includes K sets of independently acquired SAR data can be presented in the following matrix form

$$\begin{pmatrix} A^1 \\ A^2 \\ \dots \\ A^K \end{pmatrix} \begin{pmatrix} V_N \\ V_E \\ V_U \end{pmatrix} = \begin{pmatrix} \Phi^1 \\ \Phi^2 \\ \dots \\ \Phi^K \end{pmatrix} \quad or \quad \hat{A}\hat{V}_{los} = \hat{\Phi}_{obs} \tag{1}$$

where matrix A consist of time intervals between consecutive SAR acquisitions (Samsonov, 2010), vector $V = \{V_N, V_E, V_U\}$ represents unknown velocities that are to be determined and vector Φ represents observed DInSAR data.

Due to a near-polar orbital configuration of all modern space-borne SAR sensors (1) can be simplified by excluding all terms responsible for the north–south motion V_N (Samsonov & d'Oreye, 2012). This approximation is reasonable when the magnitude of north–south component of deformation is not significantly larger than the magnitude of east–west and vertical components. In this paper the magnitude of deformation is measured relative to a local reference site, which is a common approach used in InSAR studies. Large north–south and, more generally, horizontal displacements in a local reference frame usually are produced either by large earthquakes or large landslides. However, events of this magnitude did not occur in the studied region during the observation time.

Solution of Eq. (1) is found by applying the Singular Value Decomposition (SVD) and Tikhonov regularization (Tikhonov & Arsenin, 1977):

$$\begin{pmatrix} \hat{A} \\ \lambda I \end{pmatrix} \begin{pmatrix} V_E \\ V_U \end{pmatrix} = \begin{pmatrix} \hat{\Phi} \\ 0 \end{pmatrix}, \tag{2}$$

where λ is a regularization parameter that can be found, for example, using L-curve method (Hansen & O'Leary, 1993) and I is an identity matrix.

The steps constituting the MSBAS processing are presented in the flow chart diagram in Fig. 1. The first three processing steps in the left column, outlined with dashed line, are performed outside of this software. The three processing steps, outlined with a thick line, are mandatory and cannot be manipulated. The remaining processing steps, outlined with the thin boundary, can be manipulated by specifying appropriate processing flags (_FLAG).

In order to compute the two-dimensional time series of ground deformation at least two sets of InSAR data are needed, one from the ascending and one from the descending orbits. This technique, however, can efficiently handle a large number of DInSAR sets for producing results with improved temporal resolution and precision. Basic DInSAR processing is performed outside of the MSBAS software using either freely available (e.g. ROI_PAC, DORIS) or commercial (GAMMA, SARscape) packages. Differential interferograms are calculated, filtered, unwrapped and geocoded with InSAR processing software and then resampled to a common grid for all sets with, for example, the GMT scripts (http://gmt.soest.hawaii.edu). Final interferograms can be either in the angular (e.g. radian) or metric (e.g. cm or m) units, which are preserved during the MSBAS processing.

The optional pre- and post-processing steps include (i) two-dimensional (2D) high pass spatial filtering (controlled by HPF_FLAG) for removing residual orbital ramps and long wave-length atmospheric signal; (ii) offset estimation or calibration (C_FLAG) for compensating temporal and spatial variations of atmospheric parameters, including pressure, humidity, temperature, and the total electron content in the ionosphere, as well as variation in the satellite location during acquisitions; (iii) 2D low-pass spatial filtering (LPF_FLAG) for removing high-frequency noise; and (iv) one-dimensional (1D) Gaussian temporal smoothing (TAV_FLAG) applied to vertical and horizontal east–west time series independently. The topographic correction (T_FLAG) produces a joint inversion that solves for the residual topographic signal and 2D displacements and the interactive mode (I_FLAG) allows selecting and saving 2D time series of ground deformation for selected pixels to a text file. The Tikhonov regularization is controlled by R_FLAG, which is equal to λ, a regularization parameter that can be found using either the L-curve method (Hansen & O'Leary, 1993) or by trial and error.

For optimal computation the software code is implemented in C++ under Linux and linked to the high performance linear algebra LAPACK (http://www.netlib.org/lapack/) and fast Fourier transform FFTW (http://www.fftw.org/) libraries. The computational time depends on region dimensions and selected processing steps, but normally does not exceed a few (<10) minutes.

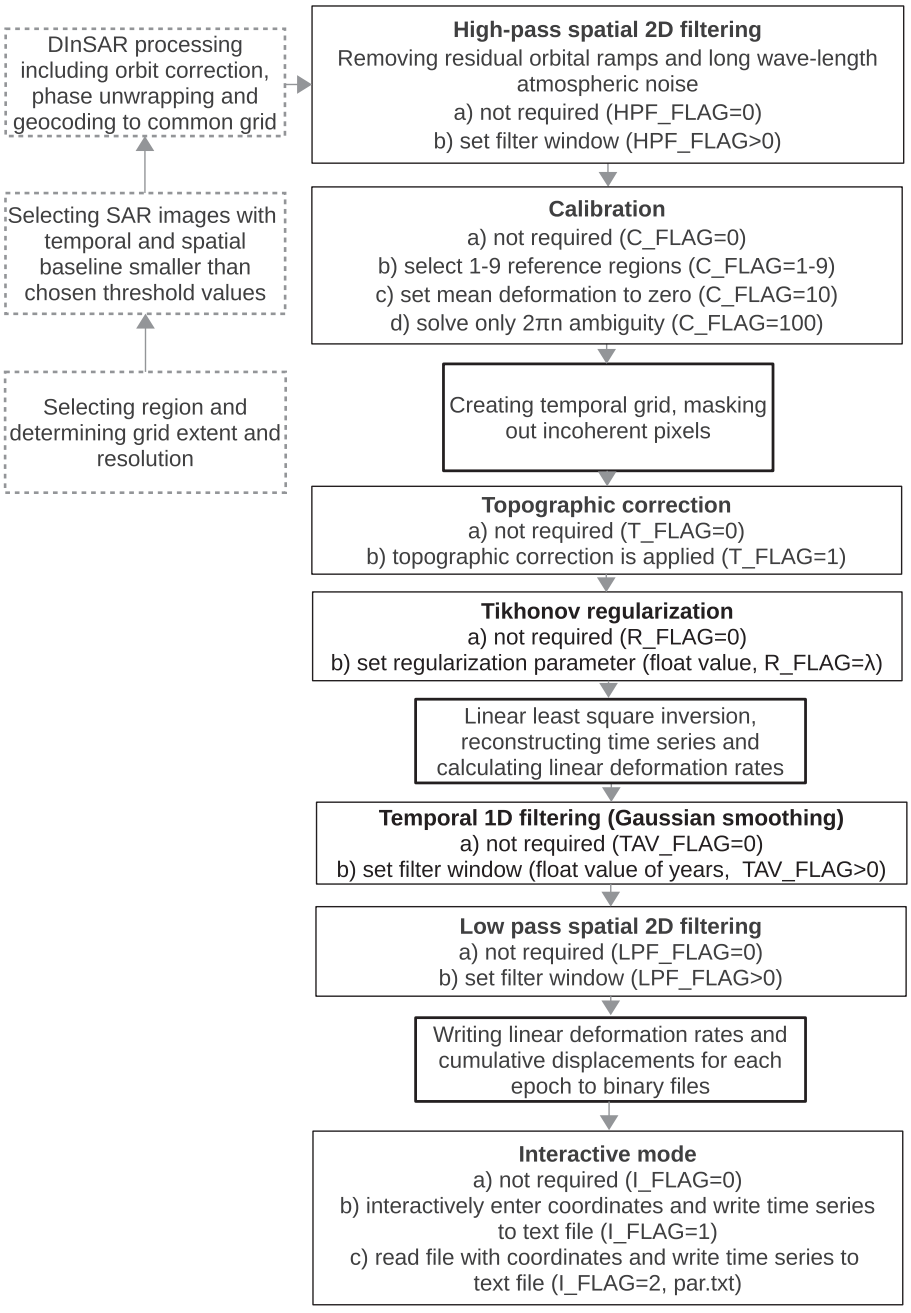

Fig. 1. Flowchart diagram of MSBAS processing algorithm. First three processing steps in left column outlined with dashed line are performed outside of this software. The three processing steps outlined with thick line are mandatory and cannot be manipulated. Remaining processing steps outlined with thin boundary can be manipulated by specifying appropriate processing flags (_FLAG).

2.1. Application to Greater Vancouver region

For achieving superior temporal resolution and precision we collected and processed a large number of SAR data consisting of seven independent sets (Fig. 3, Table 1): one ascending and one descending ERS-1/2 and ENVISAT frames, together spanning July 1995–September 2010 and three RADARSAT-2 frames spanning February 2009–October 2012. The ascending ERS-1 data from track 392, spanning 1992–1995, consisted only of a few images that later were excluded from further processing due to low coherence, therefore limiting the initial processing date to July 1995.

Each SAR data set was processed independently with GAMMA software (Wegmuller & Werner, 1997) in the following way. A single master for each set was selected and remaining images were re-sampled

Table 1
SAR data sets used in this study: ERS-1/2 and ENVISAT ascending track 392 and descending track 199, RADARSAT-2 Multi-Look Fine 21 (MF21), Fine Quad 2 (FQ2), and Fine 2 Near (F2N); time span (in YYYYMMDD format), range-azimuth resolution (extracted from SAR data headers), azimuth θ and incidence ϕ angles, number of available SAR images N (206 different acquisition dates), and number of calculated interferograms M for each data set.

InSAR set	Time span	Resolution, m	θ°	ϕ°	N	M
ERS-ENV (asc)	19950716-20080519	7.8–4.0	345	23	27	40
ERS-ENV (dsc)	19921106-20100927	7.8–4.0	−165	23	73	291
R2 MF21 (asc)	20100124-20130225	2.7–2.9	349	37	33	129
R2 FQ2 (asc)	20090219-20121025	4.7–4.9	347	23	47	236
R2 F2N (dsc)	20090321-20121031	4.7–5.2	−170	41	38	105
Total:	19950716-20121031				218	801

into the master geometry. The topographic phase was removed using the 20 m resolution DEM provided by the GeoBase (http://www.geobase.ca/) with an approximate reported elevation accuracy of 5 m. Differential interferograms were filtered using the adaptive filtering with filtering function based on local fringe spectrum (Goldstein & Werner, 1998) and unwrapped using the minimum cost flow algorithm (Costantini, 1998). The residual orbital ramp was observed in many interferograms and baseline refinement was performed to correct it. Minor interpolation of each interferogram was performed in order to increase the coverage reduced by decorrelation. This process is described in greater detail in Samsonov, Beavan, González, Tiampo, and J., F. (2011). The corrected interferograms were geocoded to the DEM grid and then re-sampled to a common lat/long grid with GMT scripts (http://gmt.soest.hawaii.edu/).

For MSBAS processing we selected 801 interferograms with the mean coherence greater than 0.5 after filtering. The large number of interferograms calculated from 218 Single Look Complex (SLC) images allowed us to achieve high precision due to the reduced impact of unwrapping, baseline errors and the tropospheric signal common to this coastal region.

The MSBAS processing was performed according to Fig. 1. We applied the 2D high-pass spatial filtering with the Gaussian impulse response function and the cut-off frequency of one pixel to remove a plane from the interferograms caused by minor errors in baseline estimation and by the long wavelength atmospheric signal. In addition to orbital and atmospheric components, the 2D high-pass spatial filtering may remove the long wavelength deformation signal produced by the subduction interplate loading processes. However, this will not affect relative ground subsidence measurements studied in this paper. Calibration was performed by subtracting a constant offset from each interferogram calculated against a single reference region that was assumed to be stable. The topographic correction was applied but 1D temporal and 2D spatial low pass filtering was not performed. The inversion was performed and vertical and horizontal east–west time series were computed. Linear deformation rates were computed by fitting a straight line to time series.

The L-curve used for selection of the regularization parameter λ is shown in Fig. 2. The λ values in range 0.12–1.00 were tested and presented in a log–log plot. For $\lambda = 0.12$ the least square or residual norm $\left\|\hat{A}\hat{V}_{los} - \hat{\Phi}_{obs}\right\|_2$ is small while the regularized or solution norm $\left\|\hat{V}_{los}\right\|_2$ is large. In the case of $\lambda = 1.00$, the residual norm is large while the solution norm is small. The value of $\lambda = 0.25$ was selected as a trade-off between both norms. Since the Eq. (2) solves for the individual deformation rates $\hat{V}_{los}$, smaller solution norm $\left\|\hat{V}_{los}\right\|_2$ means smaller absolute values of the deformation rates and, therefore, smaller cumulative ground displacements.

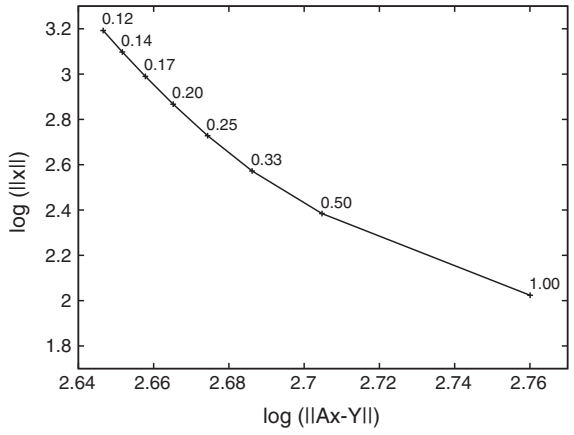

Fig. 2. L-curve for Tikhonov regularization showing trade-off between Least Square or residual norm and regularized norm for different values of regularization parameter λ ranging from 0.12 to 1.00. In this study $\lambda = 0.25$ was used.

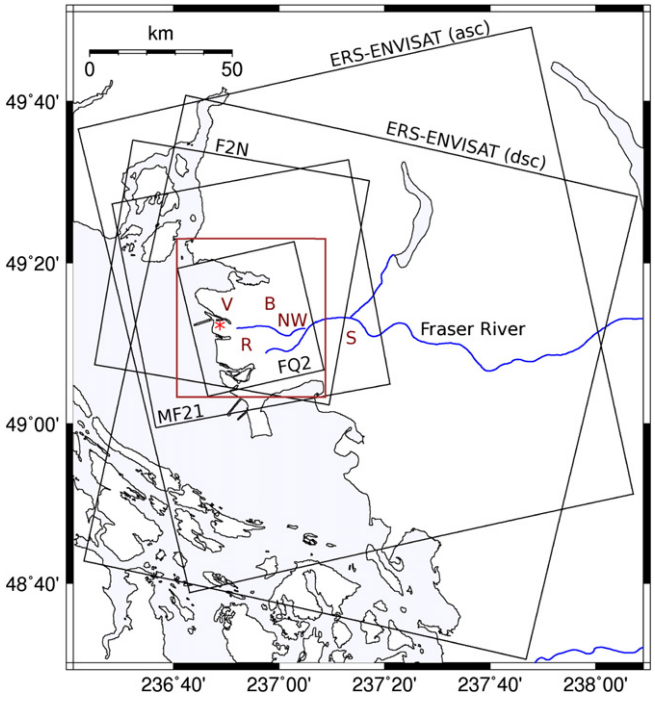

Fig. 3. Greater Vancouver region studied here is outlined in brown. In black SAR frames used in this study: RADARSAT-2 Fine Quad 2 (FQ2), Fine 2 Near (F2N), Multi-Look Fine 21 (MF21), and ERS-1/2 and ENVISAT ascending track 392 and descending track 199. Cities: B — Burnaby, R — Richmond, S — Surrey, NW — New Westminster, V — Vancouver. Red star shows location of Vancouver International Airport (YVR).

3. Results

In order to demonstrate the best possible temporal and spatial coverage we performed two runs and present here two sets of results. The first set is based on RADARSAT-2 data that spans February 2009–October 2012, shown in Figs. 4–5. The RADARSAT-2 deformation map displays improved spatial coverage due to (i) superior spatial resolution, (ii) shorter repeat time (24 days vs 36 days for ERS and ENVISAT), and (iii) smaller spatial baseline variability that in combination allowed us to produce a larger number of highly coherent interferograms over a shorter period of time. The second set is based on ERS-1/2, ENVISAT and RADARSAT-2 data that spans July 1995–October 2012 and is shown in Figs. 6–7. This deformation map has sparser spatial but longer temporal coverage.

In order to improve visualization, the deformation rate in Figs. 4 and 6 was clipped to maximum values of 0.5 cm/year. The actual values of subsidence reached 2 cm/year, which can be seen in the time series presented in Figs. 5 and 7, but the areas of fast subsidence are of very small extent.

The 2009–2012 deformation map (Fig. 4) clearly illustrates ground subsidence and the time series for points P1–P12 (P implies "partial" time period) that correspond to regions of interest are shown in Fig. 5. Points P1 and P2 coincide with the Vancouver International Airport, for which the cumulative subsidence during 2009–2012 reached almost 6 cm (Fig. 5(a) and (b)). Point P3 coincides with Terra Nova, a newest residential development on westernmost Lulu Island in Richmond and point P4 coincides with the Templeton SkyTrain transit station that was put into operation in 2009. Both these sites experienced rapid subsidence during 2009–2012. Points P5 and P6 are industrial sites, although they were agricultural a decade ago. Points P7–P9 correspond to the Iona Island, Annacis Island and Lulu Island Wastewater Treatment

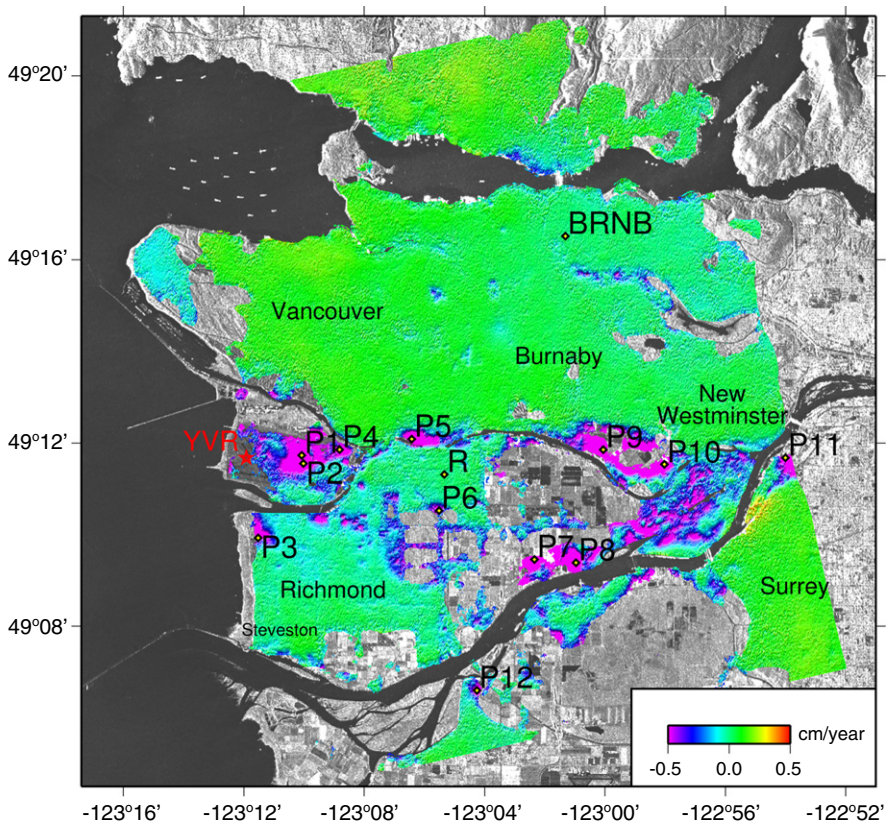

Fig. 4. RADARSAT-2 vertical linear deformation rate observed during February 2009–October 2012 and calculated with MSBAS technique. Subsidence rates were clipped for clarity to maximum values [−0.5;0.5] cm/year. For points P1–P12 (P implies "partial" time period) time series of ground deformation are presented in next figure. Cities Burnaby, Richmond, Surrey, New Westminster and Vancouver are shown. BRNB — GPS station, R — reference region considered as stable during MSBAS processing, YVR — Vancouver International Airport.

Plants. P10 and P11 correspond to the location of the Lafarge Cement Plant and point P12 corresponds to the location of the Highway 99 and Highway 91 connection ramp in Richmond. Areas of slow localized subsidence also are observed throughout the entire map, including the cities of Richmond, Vancouver, New Westminster, Surrey and Burnaby.

The deformation map spanning 1995–2012 is shown in Fig. 6. This map has a limited spatial extent and displays subsidence in similar locations to Fig. 4, but in general has a lower magnitude of less than 0.8 cm/year. Nevertheless, the subsidence rate here is slightly larger than the one reported in (Mazzotti et al., 2009). Most importantly, the subsidence is localized and does not underlie the entire city of Richmond. Time series of ground deformation are extracted for twelve points, F1–F12 (F implies "full" time period), that are precisely collocated with points P1–P12.

The 1995–2012 time series of ground deformation clearly display acceleration of subsidence beneath the Vancouver International Airport (F1, F2) and Terra Nova residential area (F3). The significant increase in the subsidence rate after 2009 is observed at points F4–F6 in northern Richmond, and a moderate increase is observed at point F7. Eastward motion is observed at points F6, F7 and F10 and westward motion is observed at points F3 and F8. Samieie-Esfahany, Hanssen, van Thienen-Visser, and Muntendam-Bos (2009) showed that horizontal motion often accompanies subsidence, although tectonic causes cannot be ruled out. However, a tectonic origin is very unlikely.

3.1. Error analysis

In order to estimate the accuracy of these measurements we performed a cross-correlation analysis, presented in Fig. 8 and in Table 2. The most reliable method for verification of DInSAR results is by comparison against independent geodetic data, usually leveling and/or GPS (e.g. Casu, Manzo, & R., L., 2006; Ferretti et al., 2007). The only readily available independent estimation of ground deformation here is a GPS three-dimensional time series from the BRNB station located in northern Burnaby (Figs. 4, 6). BRNB GPS data from the Washington State Reference Network is processed by the Pacific Northwest Geodetic Array (PANGA). The 2007–2013 vertical deformation rate at this site is −0.180.2 cm/year. Initially we selected a region around BRNB as a reference for the MSBAS processing. We observed that a region marked by point *R* (see Figs. 4, 6) uplifts during 1995–2012 with a 0.18 cm/year rate relative to BRNB, however most uplift occurs during 2004–2008. During 2009–2013 relative motion between BRNB and *R* sites is negligible (<0.02 cm/year). This allowed us to use point *R* as a reference in further processing assuming that observed at BRNB subsidence is of a regional scale. Point *R* is located in a close proximity to subsiding areas (the main objective of this study), therefore atmospheric and orbital signals proportional to the distance between the reference and measurement locations are minimized. Detrended and cleaned GPS and RADARSAT-2 MSBAS time series for BRNB site are shown in Fig. 8(a) and (b) and the standard deviations (assuming deviation from mean due to noise only) for the east–west and up–down time series are equal to 0.15 and 0.55 cm for GPS and 0.27 and 0.18 cm for RADARSAT-2 MSBAS. Therefore, horizontal motion is mapped with superior precision by GPS and vertical motion is mapped with superior precision by MSBAS InSAR.

We further calculated SBAS LOS linear deformation rates for each of five data sets (assuming here ERS-1/2 and ENVISAT as one set) and converted them to vertical deformation rates. This was done by dividing LOS measurements by $S_U = \cos\phi$ and assuming that all deformation are vertical. We extracted vertical deformation rates for twelve fast moving points from Figs. 5 and 7 and for these values estimated the correlation coefficient and the root mean square error (RMSE) between

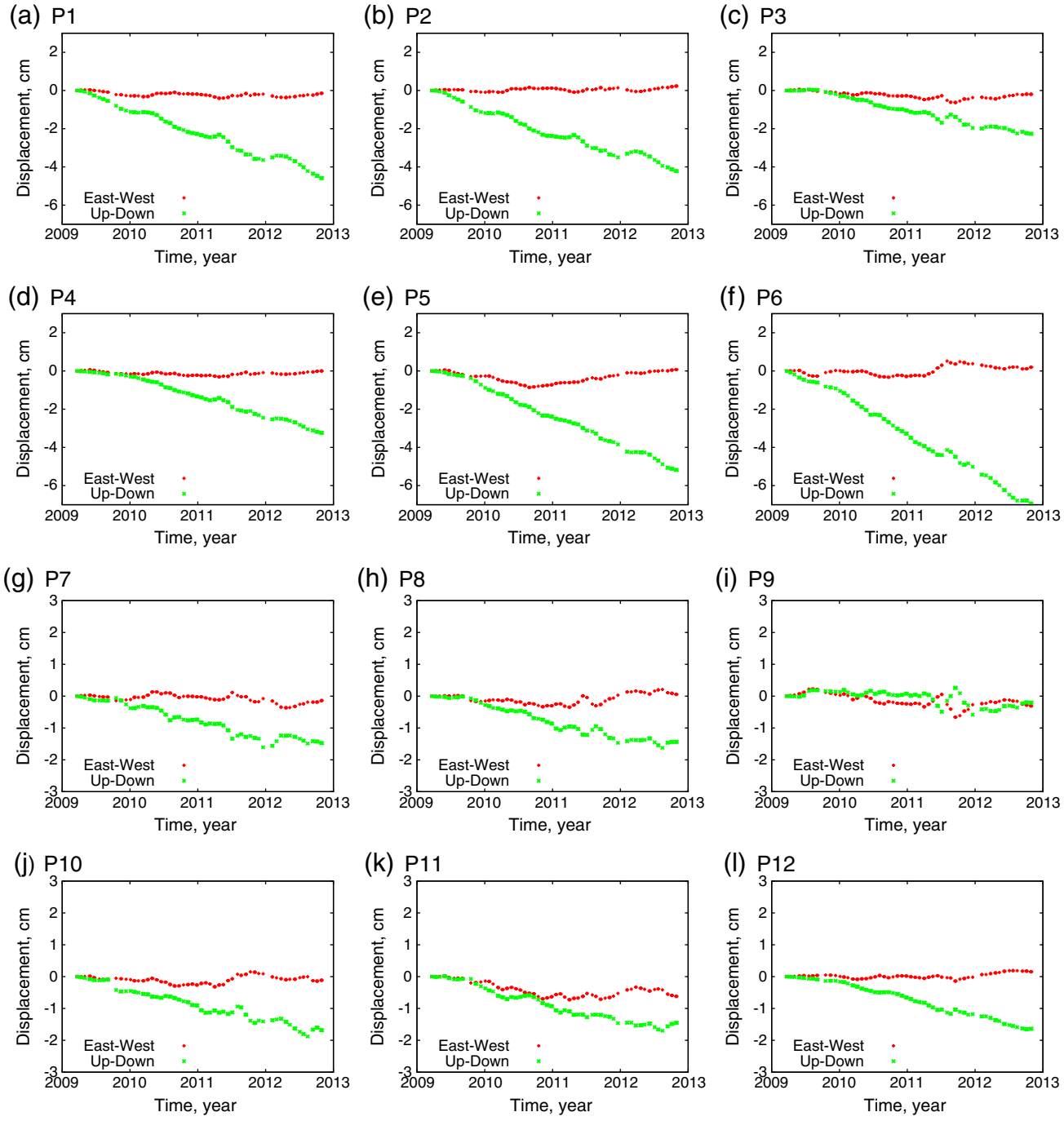

Fig. 5. RADARSAT-2 time series of ground deformation calculated for twelve points (from Fig. 4) experiencing fast subsidence. Vertical (in green) and horizontal east–west (in red) time series are shown. Note the difference in scale between (a)–(f) and (g)–(l).

five sets and MSBAS vertical deformation map. These results are reported in Table 2, while RADARSAT-2 results are reported in Fig. 8(c). For RADARSAT-2 data the correlation coefficient is 0.94–0.98 and RMSE is 0.15–0.4 cm/year; for combined ERS-ENVISAT data these values are 0.71–0.89 and 0.10–0.15 cm/year respectively.

Results of a second test for the RADARSAT-2 deformation map from Fig. 4 are shown in Fig. 8(d). Here we plotted the frequency distribution and estimated its mode. We selected only the values corresponding to the vertical motion greater than the mode of the distribution and removed the remainder. We then added the mirrored values, producing a nearly Gaussian distribution for which we estimated a standard deviation σ equal to 0.14 cm/year. Based on this calculation we concluded that the vertical deformation rate with the absolute values larger than $2\sigma = 0.28$ cm/year corresponds to the true ground deformation with probability 95% (Casu et al., 2006; Ferretti et al., 2007).

3.2. Discussion

The Greater Vancouver region, or Metro Vancouver, is located in southwestern British Columbia. It is a tectonically active region that

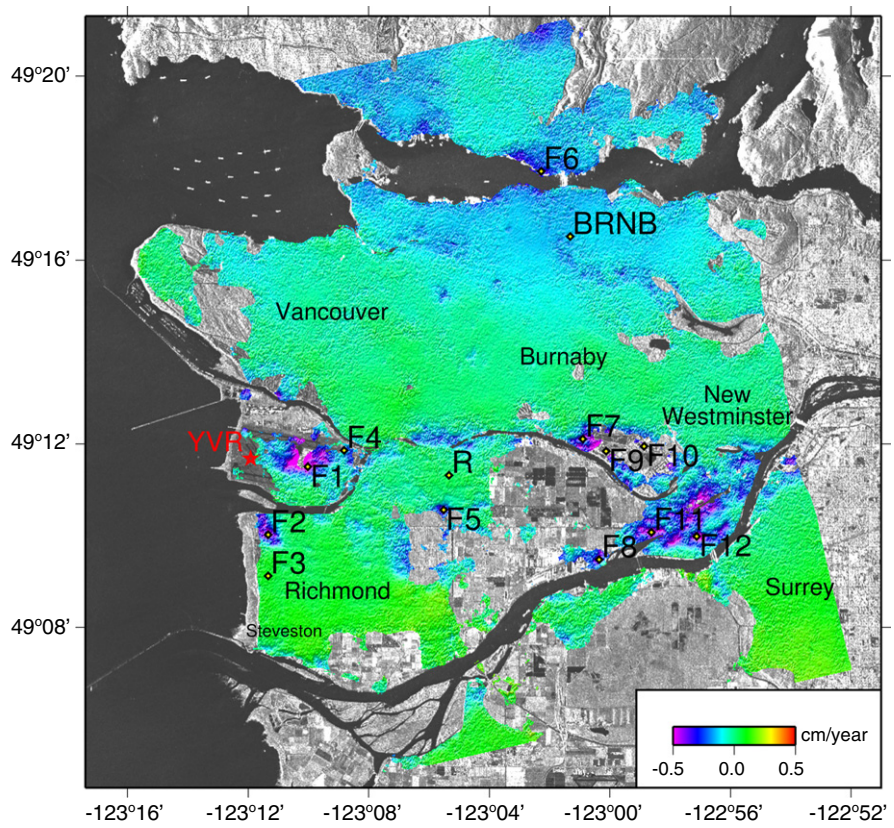

Fig. 6. ERS-ENVISAT-RADARSAT-2 vertical linear deformation rate observed during July 1995–October 2012 and calculated with MSBAS technique. Subsidence rates were clipped for clarity to maximum values [−0.5;0.5] cm/year. For points F1–F12 (F implies "full" time period) time series of ground deformation are presented in next figure. Note that these points do not precisely correspond to points in Figs. 4–5 due to difference in coverage caused by temporal decorrelation. Cities Burnaby, Richmond, Surrey, New Westminster and Vancouver are shown. BRNB — GPS station, R — reference region considered as stable during MSBAS processing, YVR — Vancouver International Airport.

was covered by the Cordilleran ice sheet during latest Pleistocene time (Clague, 1981) and is part of a large structural trough, called the Georgia Depression, that extends from south-coastal British Columbia into northwest Washington State (Mustard et al., 1998). Metro Vancouver is the third most populous metropolitan area in Canada and the largest in western Canada, with a population of 2.3 million people (http://www.statcan.gc.ca/start-debut-eng.html). Metro Vancouver comprises several separate but neighboring cities; those represented in the study are Vancouver, Richmond, Burnaby, New Westminster, and Surrey (Fig. 3).

A geologic feature in Metro Vancouver that is of importance to this study is the Fraser River Delta, which was built over the past 10,000 years in a glacio-isostatically depressed valley at the mouth of the Fraser River (Fig. 9). The Fraser Delta is considered the "largest, most populated and most important delta in western Canada" (Clague, 1998). Most of the Fraser Delta lies within the cities of Richmond and Delta (located south of the studied area), with small portions in Vancouver and New Westminster. The delta comprises Holocene sediments, mainly silts and sands, ranging up to 300 m thick. These sediments overlie thick late Pleistocene and older glacial and Tertiary bedrock (Luternauer, Harris, Hunter, & Finn, 1995). The depth of the base of the deltaic sequence varies from as little as 19 m to over 300 m below the delta plain. The Holocene sequence is thinnest and oldest in eastern (east of a reference point R in Figs. 4 and 6) Richmond and Delta. In contrast, the sequence is thickest and younger to the west. The deltaic sequence comprises, from top to bottom: (1) a thin (ca. 3–6 m) cap of fluvial and intertidal silts and peat; (2) a ca. 8–20-m thick sheet of sand deposited in distributary channels of the Fraser River at a time when sea level was lower than today; (3) up to 250 m of silts deposited on the former slope of the Fraser Delta; and (4) 10–over 100 m of prodeltaic clayey silts deposited on the floor of the Strait of Georgia (Clague, 1998; Clague, Luternauer, & Hebda, 1983; Monahan, Luternauer, & Barrie, 1993). Observed rapid subsidence in Metro Vancouver is restricted to areas underlain by Holocene sediments of the Fraser Delta.

Vancouver, Burnaby, New Westminster, and Surrey are situated on uplands underlain by thick Pleistocene sediments. In parts of Vancouver, Eocene sedimentary rocks occur at shallow depths beneath the Pleistocene cover. On the timescale of concern in this study, little or no vertical land-level change is evident in these areas.

The porous, permeable, water-saturated fine sand, silty sand, and silt that dominate the Holocene sediment sequence are compressible to considerable depth and thus are capable of producing significant settlement, especially under structural loads, dewatering, or seismic shaking. Construction of protective dikes, starting in the early 1900s, has prevented flooding and sediment deposition on the delta plain, leading to slow subsidence (Mathews & Shepard, 1962). Subsidence of 0.1–0.2 cm/year is largely related to the slow, natural consolidation of the Holocene sediment pile (Mathews & Shepard, 1962; Mazzotti et al., 2009). Localized higher rates of subsidence (settlement) stem from anthropogenic sources, notable the application of loads in construction.

Most recent rapid subsidence is localized on the shallow eastern part of the Fraser Delta, east of a reference point R in Figs. 4 and 6. Exceptions include the Vancouver International Airport (points P1/F1, P2/F2 in Figs. 4 and 6) and other areas on Sea Island and Terra Nova (P3/F3), which is a new residential development on westernmost Lulu Island in Richmond. Both the Vancouver International Airport and Terra Nova are located on thick, relatively young, Holocene sediments. In contrast, Steveston (NW of point P9/F9), which is the longest inhabited area on the Fraser Delta, shows the least amount of subsidence in Richmond.

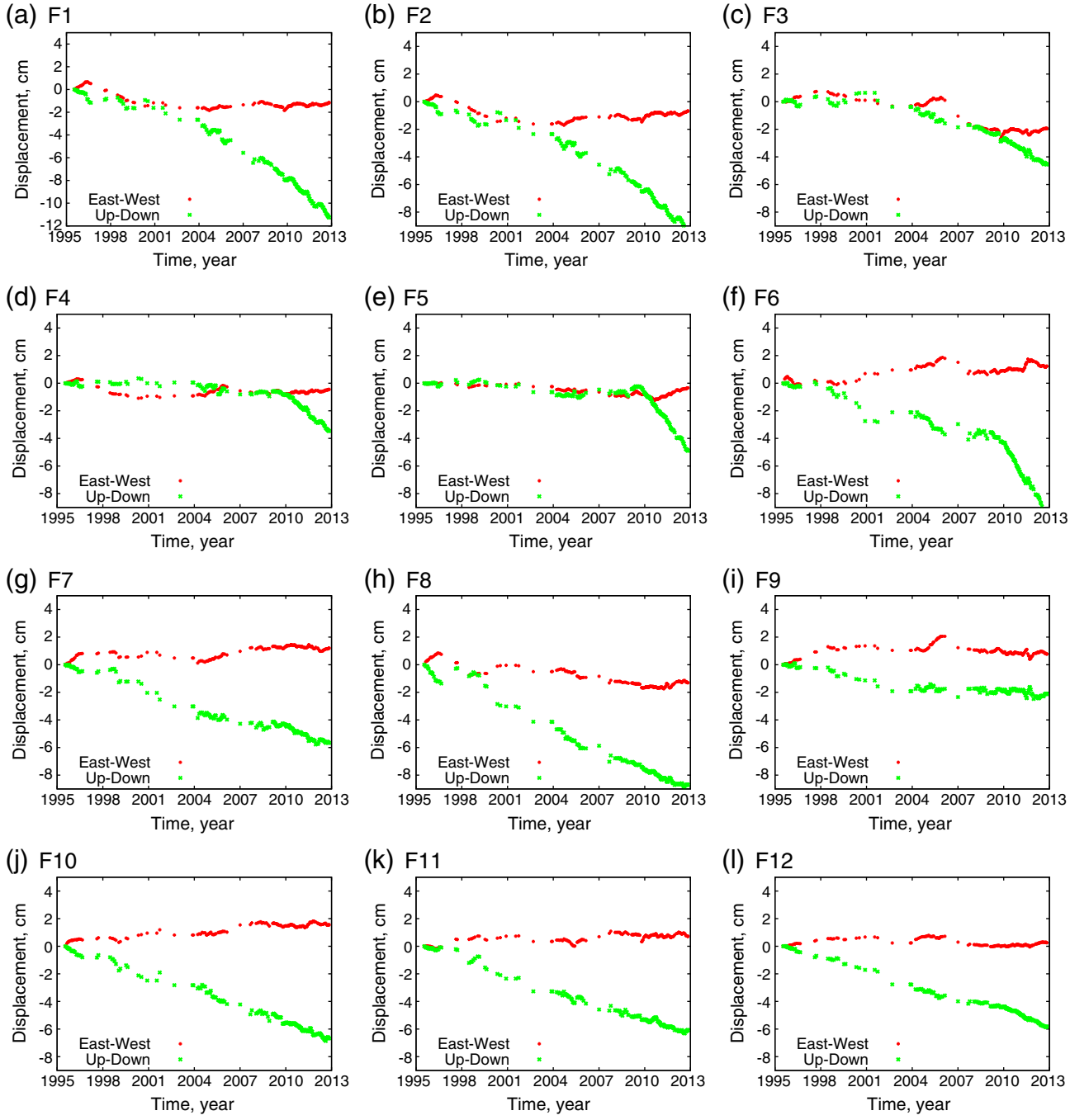

Fig. 7. ERS-ENVISAT-RADARSAT-2 time series of ground deformation calculated for twelve points (from Fig. 6) experiencing fast subsidence. Vertical (in green) and horizontal east–west (in red) time series are shown. Note different scale in (a).

Nearly all observed rapid subsidence (with a maximum rate of about 2 cm/year) is attributable to recent construction. Two exceptions are sites P12/F12 and the most eastern subsidence in northern Surrey. Areas with the largest sustained subsidence are associated with industrial sites or large commercial buildings. Two areas that are experiencing rapid subsidence, but have no large structures, are Terra Nova (P3/F3) and the Templeton SkyTrain transit station (P4/F4), which has a large parking lot and was put into service in 2009.

Mazzotti et al. (2009) found a low correlation between the rate of subsidence and the thickness of Holocene sediments on the Fraser Delta. In contrast, Ertolahti (unpublished information) found a weak, although statistically significant correlation between Holocene sediment thickness and subsidence rate on the eastern part of the Delta. Available data in western Richmond are too sparse to draw conclusions about the effect of sediment thickness on subsidence. Furthermore, no obvious relation exists between surface geology and subsidence rates. Nevertheless, much of the surface sediments on the Fraser Delta were removed prior to development, notably peat soils. In the context of deltas, Meckel, Ten Brink, and Williams (2007) argue that compaction rates may correlate poorly with cumulative subsidence of deltaic sediments, recent sedimentation rates, and the thickness and facies of the most recently deposited sediments.

Crawford and Morrison (1996) found that consolidation on the Fraser Delta occurs very rapidly in the uppermost sediments in the sequence and as the surface loads are being applied. After the uppermost sediments consolidate, deeper sediments undergo a much longer term

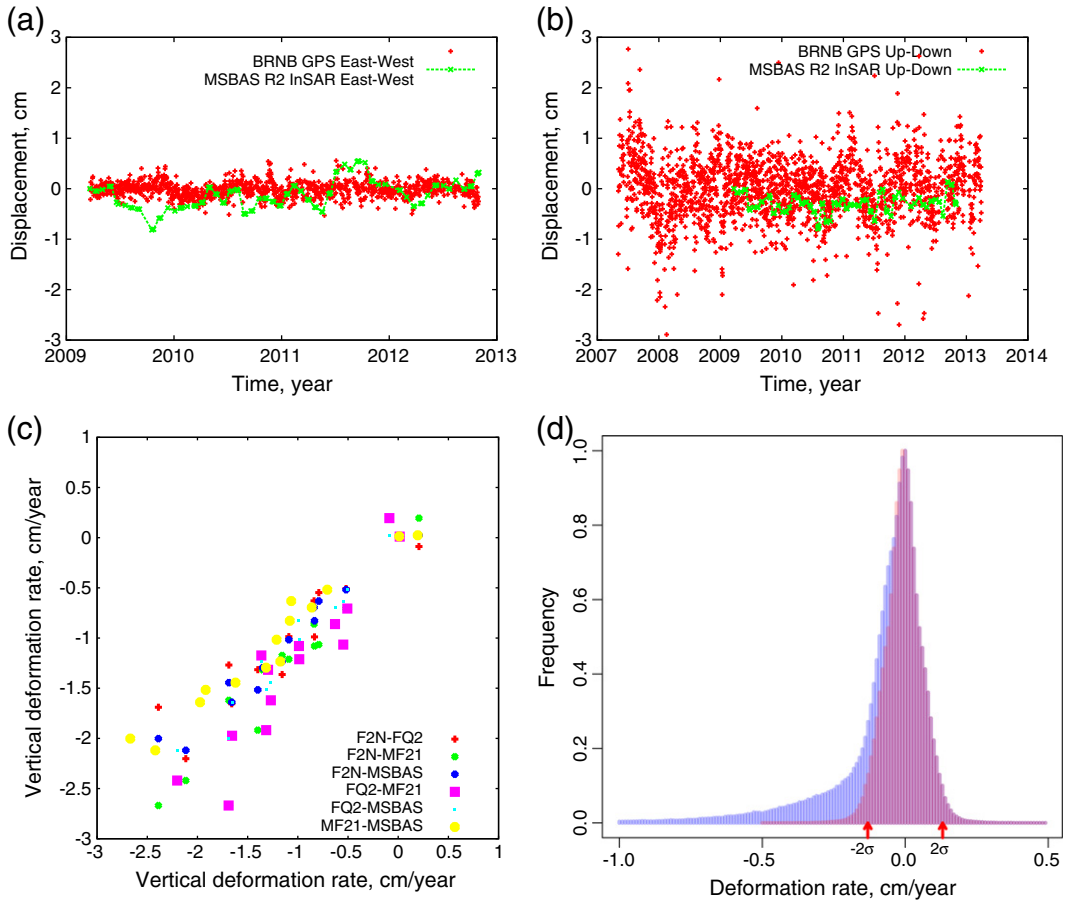

Fig. 8. (a–b) Horizontal and vertical GPS (0.15 and 0.55 cm) and MSBAS (0.27 and 0.18 cm) time series at BRNB site with corresponding standard deviation σ in brackets. (c) Correlation plots between linear deformation rates normalized by incidence angle ($1/\cos\phi$), for three independent SBAS linear deformation rates (not shown here) for each RADARSAT-2 frame and vertical component of MSBAS for twelve points from Figs. 4–5. (d) Histogram of MSBAS vertical deformation rates from Fig. 4, red arrows show 2σ (0.28 cm/year) confidence interval.

consolidation, leading to additional settlement. The rates of these deeper consolidations can be uniform irrespective of stratigraphy. Such long-term consolidation is considered to be secondary, but is difficult to predict without deep borehole data.

Our observations suggest that similar total amounts of settlement result from similar-sized loads, but subsidence rates for similar structures can differ considerably, in agreement with Meckel et al. (2007). There are three waste water treatment plants on the Fraser Delta — one on Iona Island north of the Vancouver International Airport (P7/F7), a second on Annacis Island (P8/F8), and a third on Lulu Island in southern Richmond (P9/F9). The plants on Annacis Island and Lulu Island are secondary treatment facilities. The capacity of the plant on Lulu Island was doubled in 1988, and it was upgraded to a secondary treatment plant in 1999. The Iona Island plant is a primary treatment facility that has undergone six upgrades, most recently in2001. Even though the most recent construction at all three facilities occurred within the same four-year period, the subsidence rate histories at the sites are very different, leading us to conclude that lithology affects the rate of subsidence. The Lulu Island plant (P9/F9) experienced rapid subsidence during construction, but has been subsiding at a low, near-background rate in the decade since. The Iona Island facility (P7/F7) experienced very rapid subsidence during plant upgrades. Although the rate of subsidence decreased by about 0.8 cm/year over the last decade, in comparison to the rates in the 1990s, it is still high. The Annacis Island plant (P8/F8) experienced variable rates of subsidence during construction. Subsidence is still rapid ten years after completion of the facility, but it is greater than the Lulu Island rate and less than the Iona Island rate.

The main terminal at the Vancouver International Airport (P1/F1, P2/F2) was built in the 1960s and underwent significant upgrades between 2007 and 2009, and installation of a SkyTrain transit station (P4/F4) that became fully operational in 2009. A new, northern runway was completed in 1996. Displacement rates at the main terminal may be amplified, and not decreasing, due to large amounts of groundwater extracted at the airport's three wells.

Site P5/F5 on western Mitchell Island and sites P6/F6 in south Burnaby are now completely industrial, whereas they were was almost undeveloped a decade ago. P5 has seen substantial continuous subsidence since 2010. P6/F6 has experienced periods of increased

Table 2
Correlation coefficient and root mean square error (RMSE) between normalized by incidence angle ($1/\cos\phi$) linear deformation rates for independent SBAS results (not shown here) for each RADARSAT-2 and ERS-ENVISAT beams and vertical component of MSBAS. For RADARSAT-2 we used MSBAS results for twelve points from Figs. 4–5 and for ERS-ENVISAT we used SBAS and MSBAS results (not shown here) for twelve points from Figs. 6–7.

InSAR sets	Correlation	RMSE, cm/year
ERS-ENV asc - dsc	0.71	0.15
ERS-ENV asc - MSBAS (up)	0.83	0.12
ERS-ENV dsc - MSBAS (up)	0.89	0.10
F2N-FQ2	0.94	0.26
F2N-MF21	0.98	0.23
F2N-MSBAS (up)	0.98	0.15
FQ2-MF21	0.93	0.4
FQ2-MSBAS (up)	0.98	0.13
MF21-MSBAS (up)	0.98	0.3

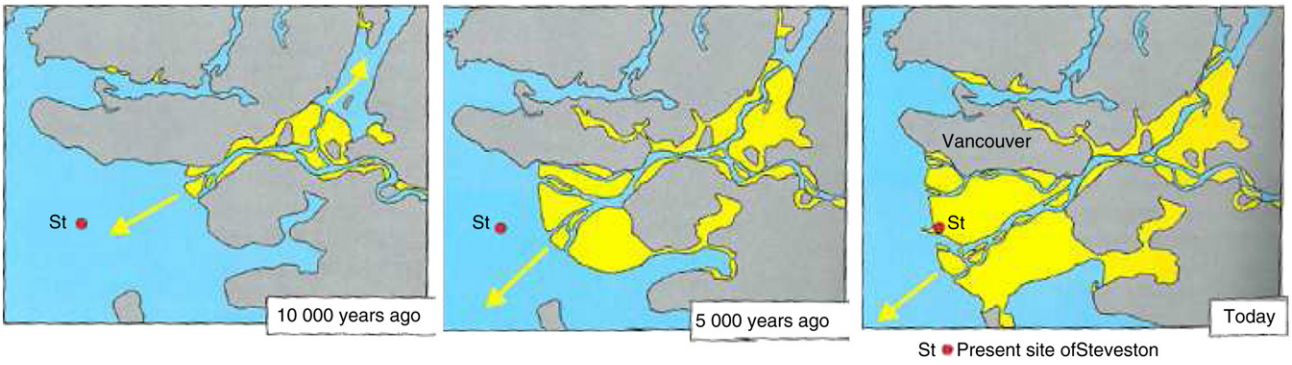

Fig. 9. Evolution of the Fraser River Delta during the Holocene (Clague & Turner, 2003). Yellow areas are Holocene sediments (floodplains, fans, and peat bogs); gray areas are pre-Holocene surfaces. Yellow arrows indicate direction of delta growth. Dates are approximate.

subsidence and then rebound, likely associated with preloading and construction. It has undergone some of the fastest subsidence observed since 2009.

The Lafarge Cement Plant sites (P10/F10 and P11/F11) have some of the most sustained, rapid subsidence of all the investigated sites. The plant was constructed in 1957, and was extensively modernized and doubled in capacity in 1999. Crawford, McCammon, and Butler (1991) studied subsidence at Lafarge and three other large plants between 1955 and 1985, and concluded that most consolidation occurs in a deep (>30 m) layer of marine sediments and is largely complete within 10 years of loading. Based on their conclusions, we would expect settlement rates today at the Lafarge site to be nearing background levels. If the InSAR data are averaged over a 400-m radius around the Lafarge plant, the subsidence rate does decrease towards background values, but point measurements on the buildings themselves indicate continuing rapid subsidence.

Settlement rates in the area surrounding the Highway 99 and Highway 91 connecting ramps in Richmond (sites P12/F12), have increased in recent years, from about 0.3 to 0.5 cm/year. The reason for this increase is unclear.

Although the effect on individual structures is a combination of a number of complex factors, differential settlement is considered a primary component when estimating potential and actual building damage (Boone, 1996). Due to the localized nature of the subsidence here, we have computed the horizontal gradient as a proxy for potential infrastructure damage index map. A maximum absolute value horizontal gradient of 0.1410^{-3} in the vertical deformation rate is observed in Fig. 10, capable of causing significant damage to local structures,

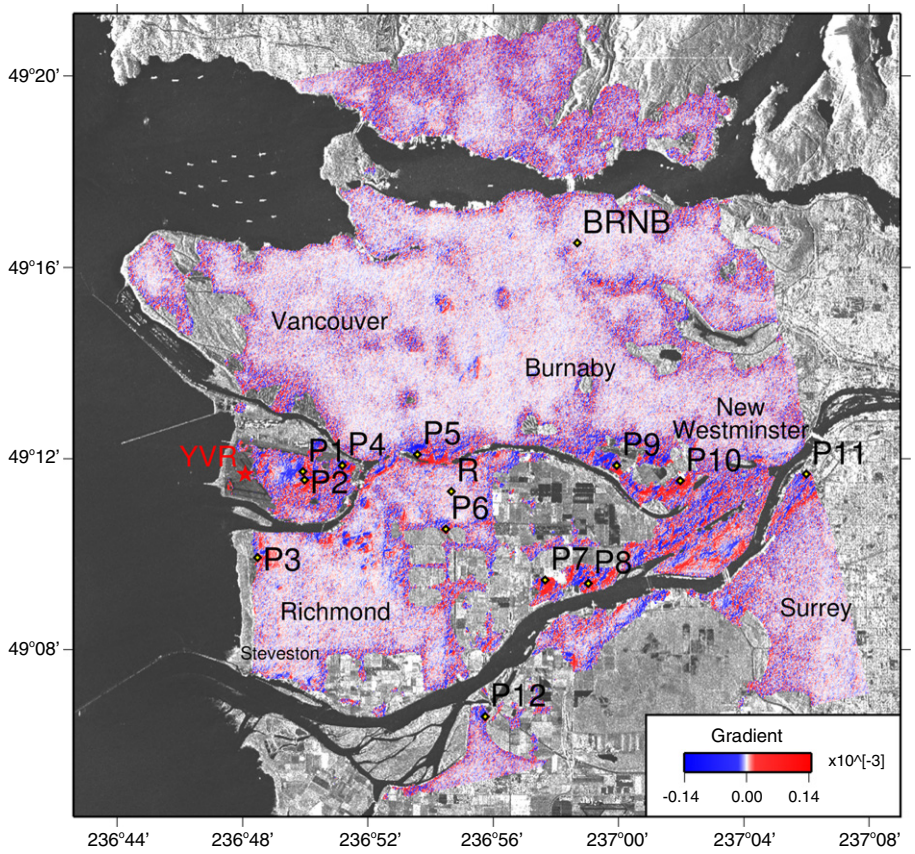

Fig. 10. Horizontal gradient of vertical linear deformation rate map calculated from RADARSAT-2 data during February 2009–October 2012 with MSBAS technique (from Fig. 4). Cities Burnaby, Richmond, Surrey, New Westminster and Vancouver are shown. YVR — Vancouver International Airport. Note that non-linear scale is used.

although more detailed studies at higher resolution are necessary to quantify the effects (Boone, 1996).

4. Conclusions

We presented the long-term vertical deformation rate maps for the Greater Vancouver region located along the Fraser River delta in the south-western part of British Columbia in Canada. For their computation we applied MSBAS method to over eight hundred ERS-1/2, ENVISAT, and RADARSAT-2 interferograms in combination spanning nearly two decades, from July 1995 until October 2012.

The 1995–2012 vertical deformation rate maps revealed widespread ground subsidence with a maximum rate of about 2 cm/year in areas underlain Holocene sediments of the Fraser Delta. In order to validate the accuracy of measurements we estimated correlation coefficient and RMSE for each SAR data set and the vertical MSBAS deformation map. We analyzed deformation rate distribution skewness that provided an alternative way for measuring precision. Both calculations suggested a very small observation error of 0.14 cm/year. It was estimated that the vertical deformation rate with the absolute values larger than $2\sigma = 0.28$ cm/year corresponds to the true ground deformation.

The localized fast subsidence was associated with a variety of different locations and construction types, including residential and industrial regions, highways and beneath the Vancouver International Airport (YVR) and SkyTrain station. At YVR the subsidence rate has been continuously increasing since 2001 while at the SkyTrain station subsidence began abruptly in 2009. The origin of subsidence is likely related to groundwater withdrawal and construction. As a proxy for a potential infrastructure damage index map we computed the horizontal gradient of the vertical deformation rate that revealed a maximum absolute value of 0.1410^{-3}, capable of causing significant damage to local structures. Detailed studies at higher resolution are necessary to quantify the impact on particular elements of infrastructure.

We demonstrate for the first time that classical time series methods with limited duration time series may lead to erroneous conclusions about the long term ground deformation. Previous studies suggested that the subsidence rates should decrease over time, therefore, reducing the impact on infrastructure. Our results show that subsidence rate is continuing to increase (due to over exploitation of groundwater and construction) and, therefore, the current anticipated impact on infrastructure is underestimated. To our knowledge, this is the first time that the same data set, complemented with new data and processed with an innovative time series method, provides the opposite conclusions: the subsidence rates in the Vancouver area is not decreasing but rather is increasing, which potentially will have important impacts on the hazard assessment for that densely populated region.

Further studies for this region using high resolution SAR data and LIDAR are warranted for estimating impact of subsidence on local structures. Improvements to this methodology also are feasible, including weighting interferograms and DInSAR sets depending on their acquisition parameters (wavelength, spatial and temporal baselines) and stochastic and seasonal parameters including atmospheric signal and land cover condition (e.g. snow coverage).

Acknowledgments

We thank the Canadian Space Agency (CSA) for providing RADARSAT-2 data and the European Space Agency (ESA) for providing ERS and ENVISAT data under projects C1P.7244 and C1P.12984. Figures were plotted with GMT and Gnuplot software and statistical analysis was performed with R software. The work of PG was supported by Banting Postdoctoral Fellowship. The work of KFT was supported by an NSERC Discovery Grant.

Appendix A. Supplementary data

Supplementary data associated with this article can be found in the online version, at http://dx.doi.org/10.1016/j.rse.2013.12.017. These data include Google map of the most important areas described in this article.

References

Berardino, P., Fornaro, G., & Lanari, R. (2002). A new algorithm for surface deformation monitoring based on small baseline differential SAR interferograms. *IEEE Transactions on Geoscience and Remote Sensing, 11*, 2375–2383.

Boone, S. (1996). Ground-movement-related building damage. *Journal of Geotechnical Engineering, 122*(11).

Casu, F., Manzo, M., & R., L. (2006). A quantitative assessment of the SBAS algorithm performance for surface deformation retrieval. *Remote Sensing of Environment, 102*, 195–210.

Clague, J. (1981). Late Quaternary geology and geochronology of British Columbia, Part 2: Summary and discussion of radiocarbon-dated Quaternary history. *Tech. Rep. Paper 80-35. Geological Survey of Canada.*

Clague, J. (1998). Geology and natural hazards of the Fraser River Delta, British Columbia. chap. *Geological setting of the Fraser River Delta. Geological Survey of Canada Bulletin, Vol. 525.* (pp. 7–16).

Clague, J., Luternauer, J., & Hebda, R. (1983). Sedimentary environments and postglacial history of the Fraser Delta and lower Fraser Valley, British Columbia. *Canadian Journal of Earth Sciences, 20*, 1314–1326.

Clague, J., & Turner, R. (2003). *Vancouver, city on the edge: Living with a dynamic geological landscape.* Vancouver, BC: Tricouni Press.

Costantini, M. (1998). A novel phase unwrapping method based on network programming. *IEEE Transactions on Geoscience and Remote Sensing, 3*, 813–821.

Crawford, C., McCammon, N., & Butler, R. (1991). Deep-seated consolidation settlements in the Fraser River Delta. *Canadian Geotechnical Journal, 28*(2), 298–303.

Crawford, C., & Morrison, K. I. (1996). Case histories illustrate the importance of secondary-type consolidation settlements in the Fraser River Delta. *Canadian Geotechnical Journal, 33*, 866–878.

Dong, S., Samsonov, S., Yin, H., Ye, S., & Cao, Y. (2013). Time-series analysis of subsidence associated with rapid urbanization in Shanghai, China measured with SBAS InSAR method. *Environmental Earth Sciences*, 1–15. http://dx.doi.org/10.1007/s12665-013-2990-y.

Ferretti, A., Novali, F., Burgmann, R., Hilley, G., & Prati, C. (2004). *InSAR permanent scatterer analysis reveals ups and downs in San Francisco Bay area, 85 (34),* EOS Transactions, AGU.

Ferretti, A., Prati, C., & Rocca, F. (2001). Permanent scatterers in SAR interferometry. *IEEE Transactions on Geoscience and Remote Sensing, 8–20.*

Ferretti, A., Savio, G., Barzaghi, A., Borghi, R., Musazzi, S., Novali, F., et al. (2007). Submillimeter accuracy of InSAR time series: experimental validation. *IEEE Transactions on Geoscience and Remote Sensing, 5–1*, 1142–1153.

Goldstein, R., & Werner, C. (1998). *Radar interferogram filtering for geophysical applications, 25 (21). (pp. 4035–4038), 4035–4038.*

Hansen, P., & O'Leary, D. (1993). The use of the L-curve in the regularization of discrete ill-posed problems. *SIAM Journal on Scientific Computing, 14*(6), 1487–1503.

Hooper, A. (2008). A multi-temporal InSAR method incorporating both persistent scatterer and small baseline approaches. *Geophysical Research Letters, 35*, 16302.

Hooper, A., Bekaert, D., Spaans, K., & Arkan, M. (2012). Recent advances in SAR interferometry time series analysis for measuring crustal deformation. *Tectonophysics, 514–517*, 1–13.

Luternauer, J., Harris, J., Hunter, J., & Finn, W. (1995). Delta geology: Hazard assessment. *The BC Professional Engineer* (pp. 11–15).

Massonnet, D., & Feigl, K. (1998). Radar interferometry and its application to changes in the Earth surface. *Reviews of Geophysics, 36*(4), 441–500.

Mathews, W., & Shepard, F. (1962). Sedimentation of Fraser River Delta, British Columbia. *American Association of Petroleum Geologists Bulletin, 1416–1443.*

Mazzotti, S., Lambert, A., van der Kooij, M., & Mainville, A. (2009). Impact of antropogenic subsidence on relative sea-level rise in the Fraser River Delta. *Geology, 37*(9), 771–774.

Meckel, T., Ten Brink, U., & Williams, S. (2007). Sediment compaction rates and subsidence in deltaic plains: Numerical constraints and stratigraphic influences. *Basin Research, 19*(1), 19–31.

Monahan, P., Luternauer, J., & Barrie, J. (1993). A delta plain sand sheet in the Fraser River Delta, British Columbia, Canada. *Quaternary International, 20*, 27–38.

Mustard, P., Clague, J., Woodsworth, G., Hickson, C., Jackson, L., Luternauer, J., et al. (1998). Urban geology of Canadian cities., vol. Special Paper 42, chap. *Geology and geological hazards of the Greater Vancouver area. Geological Association of Canada.* (pp. 39–70).

Rocca, F. (2003). 3D motion recovery with multi-angle and/or left right interferometry. *Proceeding of Fringe 2003 Workshop.*

Rosen, P., Hensley, P., Joughin, I., Li, F., Madsen, S., Rodriguez, E., et al. (2000). Synthetic aperture radar interferometry. *Proceedings of the IEEE, 88*(3), 333–382.

Samieie-Esfahany, S., Hanssen, R., van Thienen-Visser, K., & Muntendam-Bos, A. (2009). On the effect of horizontal deformation on InSAR subsidence estimates. *Fringe 2009 Workshop, ESA SP-677.*

Samsonov, S. (2010). Topographic correction for ALOS PALSAR interferometry. *IEEE Transactions on Geoscience and Remote Sensing, 7*, 3020–3027.

Samsonov, S., Beavan, J., González, P. J., Tiampo, K., & Fernández, J. (2011). Ground deformation in the Taupo Volcanic Zone, New Zealand observed by ALOS PALSAR interferometry. *Geophysical Journal International, 187*(1), 147–160.

Samsonov, S., & d'Oreye, N. (2012). Multidimensional time series analysis of ground deformation from multiple InSAR data sets applied to Virunga Volcanic Province. *Geophysical Journal International*, *191*(3), 1095–1108.

Samsonov, S., d'Oreye, N., & Smets, B. (2013). Ground deformation associated with post-mining activity at the French–German border revealed by novel InSAR time series method. *International Journal of Applied Earth Observation and Geoinformation*, *23*, 142–154.

Samsonov, S., González, P. J., & Tiampo, K. (2014). Mathematics of planet Earth (Lecture Notes in Earth System Sciences). chap. *Anthropogenic and natural ground deformation observed in Bologna region, Italy, by Radarsat-2 InSAR during 2008–2013* (pp. 383–386). Springer.

Samsonov, S., González, P. J., Tiampo, K., Camacho, A., & Fernández, J. (2014). Mathematics of planet Earth (Lecture Notes in Earth System Sciences). chap. *Spatiotemporal analysis of ground deformation at Campi Flegrei and Mt Vesuvius, Italy, observed by Envisat and Radarsat-2 InSAR during 2003–2013* (pp. 377–382). Springer.

Samsonov, S., González, P. J., Tiampo, K., & d'Oreye, N. (2013). Methodology for spatio-temporal analysis of ground deformation occurring near Rice Lake (Saskatchewan) observed by Radarsat-2 DInSAR during 2008–2011. *Canadian Journal of Remote Sensing*, *39*(1), 27–33.

Samsonov, S., González, P. J., Tiampo, K., & d'Oreye, N. (2013). Modeling of fast ground subsidence observed in southern Saskatchewan (Canada) during 2008–2011. *Natural Hazards and Earth System Sciences Discussions*, *1*, 5881–5910.

Samsonov, S., van der Koij, M., & Tiampo, K. (2011). A simultaneous inversion for deformation rates and topographic errors of DInSAR data utilizing linear least square inversion technique. *Computers and Geosciences*, *37*(8), 1083–1091.

Smets, B., d'Oreye, N., Kervyn, F., Kervyn, M., Albino, F., Arellano, S., et al. (2014). Detailed multidisciplinary monitoring reveals pre- and co-eruptive signals at Nyamulagira volcano (North Kivu, Democratic Republic of Congo). *Bulletin of Volcanology*, *76*(787), 1–35.

Syvitski, J., Kettner, A., Overeem, I., Hutton, E., Hannon, M., Brakenridge, G., et al. (2009). Sinking deltas due to human activities. *Nature Geoscience*, *2*, 681–686.

Tikhonov, A., & Arsenin, V. (1977). *Solution of ill-posed problems.* John Wiley & Sons.

Usai, S. (2003). A least squares database approach for SAR interferometric data. *IEEE Transactions on Geoscience and Remote Sensing*, *4*, 753–760.

Wegmuller, U., & Werner, C. (1997). Gamma SAR processor and interferometry software. *The 3rd ERS symposium on space at the service of our environment, Florence, Italy*.

Wright, T., Parsons, B., & Lu, Z. (2004). Toward mapping surface deformation in three dimensions using InSAR. *Geophysical Research Letters*, *31*(L01607).